Research in Astronomy and Astrophysics, 25:055016 (11pp), 2025 May
https://doi.org/10.1088/1674-4527/adce4e
CSTR: 32081.14.RAA.adce4e

Thermal Evolution of the Central Compact Object in HESS J1731−347 as Evidence for a Color-flavor-locked Strange Star

Ya-Jing Yuan[1,2] and Xia Zhou[1,3,4]
[1] Xinjiang Astronomical Observatory, Chinese Academy of Sciences, Urumqi 830011, China; zhouxia@xao.ac.cn
[2] University of Chinese Academy of Sciences, Beijing 100049, China
[3] Key Laboratory of Radio Astronomy and Technology (Chinese Academy of Sciences), Beijing 100101, China
[4] Xinjiang Key Laboratory of Radio Astrophysics, Urumqi 830011, China
Received 2025 February 25; revised 2025 April 6; accepted 2025 April 11; published 2025 May 20

Abstract

The central compact object XMMU J173203.3−344518 in the supernova remnant HESS J1731−347 challenges conventional neutron star models due to its low mass $M = 0.77^{+0.20}_{-0.17} M_{\odot}$and high redshifted surface temperature $T_s^{\infty} = 156^{+6}_{-6}$ eV ($1.81^{+0.07}_{-0.07} \times 10^6$ K). We investigate the observational properties of XMMU J173203.3−344518 within a color-flavor-locked(CFL) phase strange star model. We construct a thermal evolution model of the CFL phase strange star, along with heating due to the viscous dissipation of *r*-mode oscillations. Employing one of the most widely used quark matter equations of state, we characterize the star properties by the strange quark mass (m_s), effective bag constant ($B_{\rm eff}$), perturbative QCD correction (a_4), and pairing gap (Δ). Our analysis demonstrates that the observed properties of XMMU J173203.3344518 can be explained by *r*-mode heating with a CFL strange star, provided that the initial spin period is shorter than 18 ms. We constrain the *r*-mode saturation amplitude to 8×10^{-3}–1.4×10^{-2} and predict a current spin period of 6–9 ms for an initial period of 1 ms. This rapid rotation is consistent with the absence of detected pulsations. The *r*-mode instability window remains robust across a wide range of pairing gap values (5–200 MeV), providing a reliable framework for interpretation regardless of microscopic uncertainties. Our results support the identification of XMMU J173203.3344518 as a rapidly rotating, low-mass CFL phase strange star, demonstrating the importance of *r*-mode heating in the thermal evolution of compact objects with exotic dense matter.

Key words: stars: neutron – stars: individual (XMMU J173203.3−344518) – stars: evolution – dense matter

1. Introduction

The study of compact stars has been an important subject of modern astrophysics since the discovery of pulsars in 1967. Observations over the past few decades have shown a diverse population of these objects, with masses ranging from the canonical $\sim 1.4 M_{\odot}$ to relatively massive $\sim 2 M_{\odot}$ stars (Lattimer 2021). However, recent observations of the central compact object (CCO) XMMU J173203.3−344518 (hereafter XMMU J1732) in the supernova remnant HESS J1731−347 (Doroshenko et al. 2022) present a significant challenge to this established paradigm, exhibiting properties that lie well outside the traditionally expected range for neutron stars.

X-ray spectral analysis reveals an unusually high effective surface temperature of $T_s^{\infty} = 156^{+6}_{-6}$ eV($1.81^{+0.07}_{-0.07} \times 10^6$ K) and the age of the remnant is estimated to be between 2 and 6 kyr (Cui et al. 2016). Especially, the derived gravitational mass and radius, $M = 0.77^{+0.20}_{-0.17} M_{\odot}$ and $R = 10.4^{+0.86}_{-0.78}$ km (Doroshenko et al. 2022), place XMMU J1732 in a previously unexplored region of the mass–radius diagram. Its mass is significantly below the theoretical minimum ($\sim 1.17\, M_{\odot}$) predicted for neutron stars formed through iron core collapse (Suwa et al. 2018), suggesting that existing nuclear matter equations of state (EoSs) may require revisions. Several works discussed possible models for this low mass compact object, including strange star models (Horvath et al. 2023; Sagun et al. 2023; Di Clemente et al. 2024), neutron stars containing a core of dark matter (Sagun et al. 2023; Liu et al. 2025), and hybrid stars undergoing phase transitions to exotic matter (Laskos-Patkos et al. 2024). Additionally, some studies have suggested that XMMU J1732 could be the lightest known neutron star (Zhang et al. 2024). However, these models often face challenges in simultaneously reproducing the observed low mass, relatively small radius, and high surface temperature, without the need for additional, carefully adjusted mechanisms.

The strange quark matter hypothesis (Witten 1984), particularly the color-flavor-locked (CFL) phase (Alford et al. 1999; Alford 2001; Alford et al. 2008), offers a compelling alternative model. At sufficiently high densities, strange quark matter may exist as the CFL phase, characterized by Cooper pairing of quarks across all flavors and colors. This pairing results in a self-bound configuration where the mass scales with the radius as $M \propto R^3$ (Li et al. 1999), in contrast to traditional

neutron stars. This self-bound strange star allows for stable, sub-solar-mass configurations. Moreover, the CFL phase modifies microphysical processes, suppressing neutrino emission and specific heat, which significantly influences the thermal and rotational evolution of the star (Alford et al. 2008; Zheng et al. 2006). Therefore, the CFL strange star scenario could naturally explain the observed mass–radius relationship. Furthermore, including *r*-mode heating within the CFL phase strange star offers a self-consistent explanation for the observed high surface temperature and low mass–radius.

R-mode oscillations, driven by gravitational wave emission via the Chandrasekhar-Friedman-Schutz (CFS) instability (Chandrasekhar 1970; Friedman & Schutz 1978; Andersson 1998), are a particularly promising heating mechanism for rapidly rotating compact objects. The instability is driven by the Coriolis force. In the CFL phase, the suppressed shear and bulk viscosities allow *r*-mode to reach higher saturation amplitudes, facilitating efficient dissipation and heating (Andersson et al. 2002; Zheng et al. 2006). This makes *r*-mode a potentially dominant heating source in CFL strange stars, especially at the early stage.

In this study, we present a comprehensive investigation of XMMU J1732 within the CFL strange star framework, incorporating *r*-mode heating. Our primary objectives are to address the following key questions: (1) Can the CFL phase EoS simultaneously account for the observed mass–radius relationship and thermal properties of XMMU J1732? (2) What constraints do the observed properties place on the microscopic parameters of strange quark matter? (3) How does *r*-mode heating in the CFL phase contribute to maintaining the observed high surface temperature? To solve these questions, we combine numerical modeling of stellar structure (using the Tolman–Oppenheimer–Volkoff equations) with detailed calculations of thermal evolution and *r*-mode instability. By incorporating the latest observational constraints and carefully evaluating theoretical uncertainties in the CFL phase parameters, we aim to develop a more comprehensive understanding of the observed properties of XMMU J1732.

This paper is organized as follows: Section 2 presents the theoretical framework and methodology. Section 3 describes our numerical results and their implications for XMMU J1732. Finally, Section 4 is the conclusion and discussion.

2. Theoretical Model and Methodology

2.1. Color-flavor-locked Phase in Strange Stars

Strange stars in the CFL phase exhibit unique properties due to the formation of Cooper pairs among quarks of all flavors and colors near the Fermi surface. This pairing mechanism fundamentally alters both the EoS and the transport properties of strange quark matter. Recent studies suggest that the observed temperature of XMMU J1732 could be explained if it is a strange star in the CFL phase (Horvath et al. 2023; Sagun et al. 2023).

In the CFL phase, grand canonical potential is modified by the pairing gap, Δ (Weissenborn et al. 2011; Zhou et al. 2018):

$$\Omega_{\rm CFL} = \Omega_{\rm free} - \frac{3}{\pi^2}\Delta^2\mu_{\rm b}^2, \tag{1}$$

where $\mu_{\rm b}$ is the baryon chemical potential, and the unpaired contribution, $\Omega_{\rm free}$, is given by:

$$\Omega_{\rm free} = \sum_i \Omega_i^0 + \frac{3}{4\pi^2}(1 - a_4)\left(\frac{\mu_{\rm b}}{3}\right)^4 + B_{\rm eff}. \tag{2}$$

where Ω_i^0 represents the ideal Fermi gas contributions from each particle species ($i = u, d, s, e$). The second term includes perturbative QCD corrections to $\mathcal{O}(a_4)$, where a_4 is a dimensionless parameter that characterizes the strength of these corrections (Alford et al. 2005). The effective bag constant, $B_{\rm eff}$, accounts for non-perturbative QCD effects. Specific values for the strange quark mass ($m_{\rm s}$), $B_{\rm eff}$, a_4, and the CFL pairing gap (Δ) are discussed in Section 3.1.

2.2. R-mode Instability in CFL Phase Strange Stars

R-mode oscillation is a non-radial oscillation in rotating stars driven by the Coriolis force and can be amplified by gravitational radiation through the CFS mechanism (Chandrasekhar 1970; Friedman & Schutz 1978; Andersson 1998). In the CFL phase of quark matter, *r*-modes are particularly significant due to the drastically reduced viscosity. The temporal evolution of these modes is governed by two coupled equations for the *r*-mode amplitude, α, and the stellar angular velocity, Ω (Owen et al. 1998; Zheng et al. 2006):

$$\frac{d\alpha}{dt} = -\alpha\left(\frac{1}{\tau_{\rm GR}} + \frac{1 - \alpha^2 Q}{\tau_{\rm v}} - \frac{1}{2\tau_{\rm m}}\right), \tag{3}$$

$$\frac{d\Omega}{dt} = -\Omega\left(\frac{2\alpha^2 Q}{\tau_{\rm v}} + \frac{1}{\tau_{\rm m}}\right). \tag{4}$$

where $\tau_{\rm GR}$, $\tau_{\rm v}$, and $\tau_{\rm m}$ represent the timescales for gravitational radiation, viscous damping and magnetic braking, respectively. The parameter $Q = 3\tilde{J}/2\tilde{I}$ quantifies the coupling between *r*-mode oscillations and bulk rotation, where $\tilde{J}$ and $\tilde{I}$ are the normalized angular momentum and moment of inertia, respectively (Ho & Lai 2000). In this work, we calculate $\tilde{J}$ and $\tilde{I}$ self-consistently using the EoS presented in Section 2.1. In the CFL phase, electron-electron scattering dominates the viscous dissipation, as other processes are exponentially suppressed by the pairing gap. This reduction in viscosity has important implications for *r*-mode and thermal evolution of the star.

The *r*-mode saturation amplitude, $\alpha_{\rm sat}$, is another key but highly uncertain parameter. While early theoretical studies proposed values near unity (Andersson 1998), more recent nonlinear analyses have significantly lowered these estimates.

Mode coupling calculations suggest $\alpha_{\rm sat}$ values in the range 10^{-4}–10^{-2}, whereas turbulent dissipation models indicate even smaller values, down to 10^{-6}–10^{-3} (Bondarescu et al. 2009). The value of $\alpha_{\rm sat}$ strongly influences both the spin-down rate and thermal evolution of the star (Atta & Basu 2025).

2.3. Thermal Evolution with R-mode Heating

The thermal evolution of XMMU J1732 follows the energy balance equation (Zheng et al. 2006):

$$C\frac{dT}{dt} = -L_{\rm neutrino} - L_{\rm photon} + H_{\rm sv}, \tag{5}$$

where C is the total specific heat, $L_{\rm neutrino}$ represents the neutrino luminosity, $L_{\rm photon}$ is the surface photon luminosity, and $H_{\rm sv}$ denotes the heating rate due to shear viscosity. In the CFL phase, pairing effects significantly suppress the specific heat, C (Blaschke et al. 2000):

$$c_{\rm sq} = 3.2c_{\rm q}(T_{\rm c}/T)\exp(-\Delta/T) \times [2.5 - 1.7T/T_{\rm c} + 3.6(T/T_{\rm c})^2]. \tag{6}$$

where $T_{\rm c}$ is the critical temperature for the CFL phase transition, Δ is the pairing gap, and $c_{\rm q}$ is a constant related to the specific heat of unpaired quark matter. These parameters influence both microscopic processes and macroscopic evolution timescales.

Within strange quark matter, three primary neutrino emission processes are typically considered: direct Urca, modified Urca, and quark bremsstrahlung (Iwamoto 1982). The corresponding neutrino emission rates per unit volume are (Zheng et al. 2006):

$$\dot{E}^{\rm (D)}_{\rm neutrino} = 8.8 \times 10^{26}\alpha_{\rm c}\left(\frac{\rho_{\rm b}}{\rho_0}\right)Y_{\rm e}^{1/3}T_9^6 \ {\rm erg\ cm^{-3}\ s^{-1}}, \tag{7}$$

$$\dot{E}^{\rm (M)}_{\rm neutrino} = 2.83 \times 10^{19}\alpha_{\rm c}^2\left(\frac{\rho_{\rm b}}{\rho_0}\right)T_9^8 \ {\rm erg\ cm^{-3}\ s^{-1}}, \tag{8}$$

$$\dot{E}^{\rm (B)}_{\rm neutrino} = 2.98 \times 10^{19}\left(\frac{\rho_{\rm b}}{\rho_0}\right)T_9^8 \ {\rm erg\ cm^{-3}\ s^{-1}}. \tag{9}$$

where $\alpha_{\rm c}$ is the strong coupling constant, $\rho_{\rm b}$ is the baryon number density, ρ_0 is the nuclear saturation density, $Y_{\rm e}$ is the electron fraction, and T_9 is the temperature in units of 10^9 K (8.6×10^4 eV).

The CFL pairing gap, Δ, plays a crucial role in both the cooling and heating processes. It exponentially suppresses neutrino emission - direct Urca by a factor of $\propto e^{-\Delta/k_BT}$, and modified Urca and quark bremsstrahlung by $\propto e^{-2\Delta/k_BT}$ (Blaschke et al. 2000) and it modifies the shear viscosity by $\propto e^{\Delta/3k_BT}$. Therefore, Δ is a critical parameter for determining the long-term thermal evolution of the star. The observed properties of XMMU J1732 need a careful treatment of these modified cooling rates and shear viscosity. While the effective bag constant, $B_{\rm eff}$, and the perturbative QCD correction, a_4, influence the stellar structure and, consequently, the r-mode coupling strength, Q, their impact is secondary (Zheng et al. 2006; Zhou et al. 2018). Over long timescales ($t \gtrsim 10^4$ yr), initial conditions become less significant, except when considering r-mode heating (Zheng et al. 2006; Zhou et al. 2018).

The relationship between the surface temperature $T_{\rm s}$ and the internal temperature T is given by Gudmundsson et al. (1983):

$$T_{\rm s} = 3.08 \times 10^6 g_{\rm s,14}^{1/4} T_9^{0.5495} \ {\rm K}, \tag{10}$$

where $g_{\rm s,14}$ is the surface gravity in units of 10^{14} cm s^{-2}:

$$g_{\rm s,14} = 1.33 \times 10^{14}\left(\frac{M}{M_\odot}\right) R_6^{-2}\left[1 - 0.295\left(\frac{M}{M_\odot}\right)R_6^{-1}\right]^{-1/2}, \tag{11}$$

where R_6 is the stellar radius in units of 10 km. Equation (10) is based on models of heat transport in neutron star envelopes composed primarily of iron (Gudmundsson et al. 1983). Although the envelope composition in a CFL strange star may differ (e.g., potentially containing a crust of normal matter or electrons), this relation remains a widely used and reasonable approximation for connecting internal and surface temperatures. While deviations could arise from detailed envelope physics specific to CFL stars, such effects are not expected to alter the overall conclusions regarding the necessity of an internal heating mechanism.

The observed high temperature of the CCO XMMU J1732 at its young age (∼2–6 kyr) requires ongoing heating beyond standard cooling. Several heating mechanisms have been proposed for compact stars, but most are not compatible with the properties of XMMU J1732. Fallback accretion is disfavored by the lack of infrared excess and the predominantly thermal X-ray spectra observed in CCOs (Wang et al. 2007; de Luca 2008). Deep crustal heating requires a past accretion episode, which is absent in these isolated objects (Brown 1999), and is primarily relevant for recycled millisecond pulsars or low mass X-ray binaries. Internal ohmic dissipation is also likely inefficient due to the relatively low surface magnetic fields inferred for CCOs ($B \sim 10^{10}$–10^{11} G) (Gotthelf et al. 2013; Viganò et al. 2013; Halpern & Gotthelf 2015).

This makes internal heating from rotational energy dissipation, particularly via the r-mode instability (Andersson 1998; Zheng et al. 2006), as the most plausible mechanism. R-mode heating is intrinsic to rapidly rotating young neutron stars and is expected to be especially efficient in the CFL phase (Andersson et al. 2002). This process naturally connects thermal emission to the dense matter EoS and aligns with the non-detection of pulsations. We therefore adopt r-mode heating as the primary mechanism driving the thermal evolution of XMMU J1732. The heating rate due to shear

viscosity is given by:

$$H_{\rm sv} = \frac{2\tilde{E}}{\tau_{\rm sv}}, \tag{12}$$

where $\tilde{E} = \frac{1}{2}\alpha^2 \tilde{J} M R^2 \Omega^2$ is the canonical energy of the r-mode. In the CFL phase, viscous dissipation from quark reactions is exponentially suppressed due to the pairing gap. As a result, shear viscosity from electron-electron scattering becomes the dominant damping mechanism (Zheng et al. 2006), with the damping timescale given by

$$\tau_{\rm sv}^{\rm ee} = 2.95 \times 10^7 \left(\frac{\mu_e}{\mu_q}\right)^{-\frac{14}{3}} T_9^{\frac{5}{3}}. \tag{13}$$

where μ_e and μ_q are the electron and quark chemical potentials, respectively.

3. Numerical Results

3.1. Model Parameters and Physical Constraints

Our numerical analysis of the thermal evolution of XMMU J1732 requires a careful selection of both microscopic and macroscopic parameters. The microscopic parameters describe the physical properties of CFL strange quark matter, while the macroscopic parameters govern the star's initial conditions and its subsequent evolution. These parameters are chosen based on theoretical constraints, alignment with recent astrophysical observations, and consistency with the measured properties of XMMU J1732 itself (Doroshenko et al. 2022), including its estimated age of 2–6 kyr (Cui et al. 2016).

The microscopic parameters determine the EoS and transport characteristics of matter in the CFL phase (Section 2.1). However, not all of them significantly influence long-term thermal evolution (Section 2.3). Wang et al. (2019) showed that, for a given mass, variations in CFL EoS parameters have only a limited effect on r-mode instability. Accordingly, we fix the strange quark mass $m_{\rm s}$, the effective bag constant $B_{\rm eff}^{1/4}$, and the perturbative QCD correction parameter a_4. We adopt $m_{\rm s} = 93$ MeV, in agreement with recent lattice QCD results and the Particle Data Group compilations (Group et al. 2022). For the effective bag constant, we choose $B_{\rm eff}^{1/4} = 144.3$ MeV, a value that ensures absolute stability of strange quark matter while reproducing the mass–radius relation of XMMU J1732 and satisfying the two-solar-mass constraint from observed pulsars. We use $a_4 = 0.55$, consistent with prior spin-based constraints (Zhou et al. 2018), NICER data (Li et al. 2021), and the upper bound inferred from GW190814 (Oikonomou & Moustakidis 2023). These parameters have only a moderate impact on global stellar properties such as mass, radius, and moment of inertia. Therefore, we fix them in our analysis to focus on the effects of the pairing gap and initial spin.

The CFL pairing gap Δ is the most uncertain microphysical parameter and plays a key role in determining both the neutrino emissivity (Equations (7)–(9)) and viscous damping, which together control the effectiveness of r-mode heating. Theoretical estimates of Δ span a wide range, and current observational constraints remain highly model dependent (Miller et al. 2019; Riley et al. 2019; Li et al. 2021; Kurkela et al. 2024). A primary goal of this study is to investigate how variations of Δ affect thermal evolution. Therefore, we explore values from 5 MeV (weak pairing) to 200 MeV (strong pairing), covering the whole range of physically plausible scenarios.

Figure 1 presents mass–radius relations for CFL strange stars using the EoS parameters discussed above. Results are shown for $\Delta = 5$ MeV and $\Delta = 200$ MeV, representing the lower and upper limits of our parameter space. For comparison, we include two representative hadronic EoSs ((DDME2 and SKI6) with mass–radius constraints for PSR J0030+0451, PSR J0437 −4715 and PSR J0740+6620. The observational constraints for XMMU J1732 and GW170817 are also shown.

As seen in Figure 1, the CFL strange star model naturally accommodates the mass–radius properties of XMMU J1732. The inferred mass ($M = 0.77^{+0.20}_{-0.17} M_\odot$) and radius ($R = 10.4^{+0.86}_{-0.78}$ km) lie within the predicted parameter space. This supports the hypothesis that XMMU J1732 could be a CFL strange star rather than a conventional neutron star. A special feature of the CFL model is the scaling relation $M \propto R^3$, which arises from the self-bound nature of strange quark matter, in contrast to the more intricate behavior associated with hadronic EoSs. The pairing gap Δ affects both the shape of the mass–radius curve and the maximum mass supported by the star.

A larger pairing gap exponentially suppresses neutrino cooling and increases shear viscosity, which is proportional to $e^{\Delta/3k_{\rm B}T}$ in the CFL phase. These effects strongly influence the star's thermal history. One of our key objectives is to constrain Δ by comparing the model predictions with the observed thermal state of XMMU J1732. The electron chemical potential μ_e is not a free parameter but is calculated self-consistently for each EoS set by enforcing charge neutrality and chemical equilibrium within the CFL phase. For the considered parameter range, we obtain $\mu_e \approx 180$ MeV.

The macroscopic parameters define the initial state and overall properties of the star. We use the observed mass, radius and redshifted surface temperature of XMMU J1732 as constraints. The initial temperature is set to $T_0 = 10^{10}$ K (8.6×10^5 eV), representative of a newly formed hot neutron star. The initial r-mode amplitude is chosen as $\alpha_0 = 10^{-10}$, which is small enough to avoid influencing early evolution while allowing us to trace the growth of r-modes (Zheng et al. 2006).

We assume a magnetic field strength of $B = 10^{11}$ G, consistent with estimates for CCOs (Halpern & Gotthelf 2015; Gotthelf et al. 2024). Although magnetic effects are not explicitly included in our simulations, they could influence

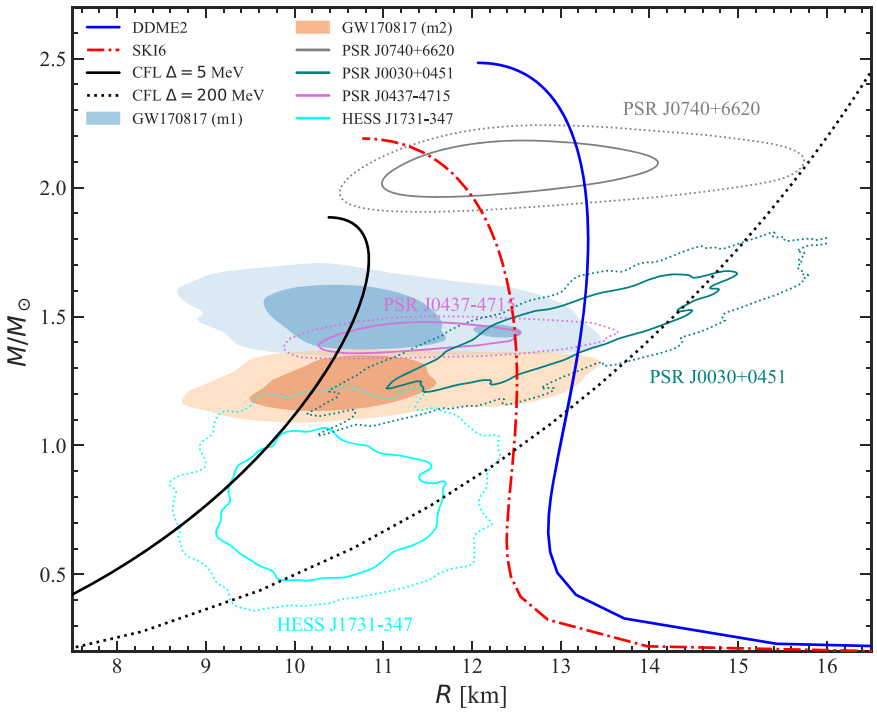

Figure 1. Mass–Radius (*M-R*) relations for CFL strange stars compared with representative hadronic EoSs and astrophysical constraints. The solid and dotted black lines show the stable CFL phase EoS with pairing gaps $\Delta = 5$ MeV and $\Delta = 200$ MeV, respectively. For comparison, the nuclear EoS models DDME2 (solid blue line) and SKI6 (dashed–dotted red line) are shown, which come from Zhou et al. (2021). Shaded regions represent the 50% (darker shade) and 90% (lighter shade) credible regions for the component masses (m1: blue, m2: orange) of GW170817 (Abbott et al. 2018). Lines are observational constraints from PSR J0740+6620 (gray) (Salmi et al. 2024), PSR J0030+0451 (teal) (Riley et al. 2019, 2021; Miller et al. 2019, 2021), PSR J0437−4715 (orchid) (Choudhury et al. 2024), and HESS J1731−347 (cyan) (Doroshenko et al. 2022). Solid and dotted lines for these objects represent the 68% and 95% credible boundaries, respectively.

r-mode damping through magnetic braking or enhanced viscous dissipation (Ho & Lai 2000; Rezzolla et al. 2000; Glampedakis et al. 2006; Wang & Dai 2017).

The initial spin period P_0 of a newborn compact star is uncertain and likely depends on its formation mechanism (Faucher-Giguere & Kaspi 2006; Lorimer 2008). The initial period of PSR B0531+21 (Crab) is estimated to be ∼19 ms (Lyne et al. 1993) (see also Sun et al. 2024 for recent discussion). Huang et al. (2022) showed that explaining the temperature of PSR B0950+08 with roto-chemical heating would require an unrealistically short $P_0 \lesssim 17$ ms. In addition, Du et al. (2024) analyzed young pulsars in supernova remnants (correcting for beaming bias) and concluded that the initial spin distribution peaks near 50 ms. These studies support a wide distribution of initial periods. To examine the influence of initial rotation on the *r*-mode heating, we consider P_0 ranging from 1 to 20 ms.

Table 1 summarizes the full set of parameters used in this study, grouped into microscopic EoS inputs, observational constraints, simulation initial conditions, and derived *r*-mode quantities. These parameters form the basis for our modeling of *r*-mode instability, thermal evolution, and quasi-equilibrium states. The normalized angular momentum $\tilde{J} = 0.033$, calculated self-consistently from the EoS, determines the strength of *r*-mode coupling and directly influences the results shown in Figures 3–5. The parameters m_s, $B_{\rm eff}$ and a_4 define the stellar structure, while Δ primarily controls neutrino emission rate and the early thermal evolution, as shown in Figure 3(a).

3.2. R-*mode Instability Window of XMMU J1732*

To evaluate the conditions under which *r*-mode oscillations become unstable in XMMU J1732, we analyze the *r*-mode instability window. This window is defined by the competition between gravitational radiation, which drives *r*-mode growth, and viscous dissipation, which suppresses it (Andersson et al. 2002). The onset and extent of the instability window are sensitive to the star's internal temperature and the properties of the CFL phase, particularly the pairing gap Δ.

Shear viscosity plays a dominant role in damping *r*-modes and is strongly affected by Δ. A larger pairing gap enhances the shear viscosity, thereby reducing the growth rate of *r*-modes. To quantify this behavior, we compute the *r*-mode instability window for several pairing gap values ($\Delta = 5$, 10, 50, 100, 150, and 200 MeV), using the EoS described in

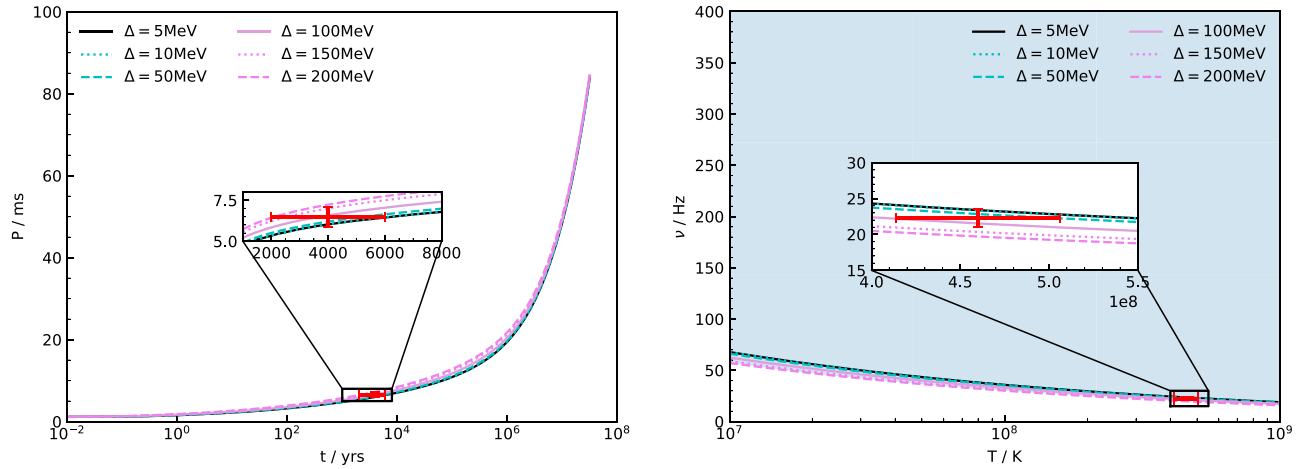

Figure 2. Spin evolution and *r*-mode instability window for XMMU J1732. (a) Spin evolution curves for different pairing gap values (Δ ranging from 5 to 200 MeV) with an initial spin period of $P_0 = 1$ ms. The error bar indicates the age constraint (2–6 kyr) and the corresponding predicted spin period range (6–9 ms). (b) *R*-mode instability windows (shaded areas) for different pairing gap values. The error bar shows the inferred internal temperature, $T = 4.6^{+0.46}_{-0.46} \times 10^8$ K ($4^{+0.4}_{-0.4} \times 10^4$ eV), and the critical frequency range, $\nu_c = 22.25^{+1.24}_{-1.24}$ Hz. The semi-analytical expression for the critical frequency, $\nu_c \approx -29.8 \log T + 280.4$ Hz, is derived from a curve fit to the numerically determined instability window boundaries.

Table 1
Model Parameters and Observational Constraints for XMMU J1732

Microscopic Parameters		Observational Constraints	
Strange quark mass (m_s)	93 MeV	Mass (M)	$0.77^{+0.20}_{-0.17} M_\odot$
Effective bag constant ($B_{\rm eff}^{1/4}$)	144.3 MeV	Radius (R)	$10.4^{+0.86}_{-0.78}$ km
Perturbative QCD correction (a_4)	0.55	Surface temperature (T_s^∞)	156^{+6}_{-6} eV
Pairing gap range (Δ)	5–200 MeV	Age	2–6 kyr
Initial Conditions		**Derived *R*-mode Parameters**	
Initial temperature (T_0)	10^{10} K	Critical frequency (ν_c)	$22.25^{+1.24}_{-1.24}$ Hz
Initial *r*-mode amplitude (α_0)	10^{-10}	Critical period (P_c)	$44.94^{+4.49}_{-4.49}$ ms
Initial spin period range (P_0)	1–18 ms	Heating rate (H_{sv})	1.27×10^{34} erg s^{-1}
Magnetic field (B)	10^{11} G	Normalized angular momentum ($\tilde{J}$)	0.033

Note. (1). The microscopic parameters characterize the CFL strange quark matter EoS. Observational constraints are from Doroshenko et al. (2022) and Cui et al. (2016). Initial conditions represent typical values for newly formed compact objects. (2). For thermal evolution simulations shown in Figures 3–5, we used $\Delta = 100$ MeV as our reference value. 3. The derived *r*-mode parameters represent calculated values based on the observed surface temperature and the theoretical model. The heating rate is calculated at the current equilibrium state and corresponds to the observed thermal luminosity of $10.8^{+3.7}_{-3.0} \times 10^{33}$ erg s^{-1}.

Section 2.1. The relevant timescales are the gravitational radiation timescale $\tau_{\rm GR}$ and the shear viscosity timescale $\tau_{\rm sv}$.

Figure 2(a) shows the spin evolution of the star assuming an initial spin period of $P_0 = 1$ ms (as specified in Table 2). The results indicate that the spin-down rate is only weakly dependent on Δ, suggesting that the loss of angular momentum via *r*-mode emission is relatively insensitive to the pairing gap across the explored parameter range. From the same figure, we estimate the current spin period of XMMU J1732 to be in the range $P = 6$–9 ms, consistent with its inferred age and assuming *r*-mode driven spin evolution.

Using the model parameters listed in Table 1, we calculate the *r*-mode instability windows for CFL strange stars across different Δ. Figure 2(b) shows the instability windows along with corresponding spin evolution curves. The shaded regions represent the temperature-frequency parameter space where *r*-

Table 2
Theoretical Predictions for Different Initial Spin Periods P_0

Fixed Parameters	Initial Period P_0 (ms)	Saturation Amplitude $\alpha_{\rm sat}$	Current Period[a,b]		Equilibrium Temperature $T_{\rm s}^{\infty}$ (K)
			$P_{\rm min}$ (ms)	$P_{\rm max}$ (ms)	
$B_{\rm eff}^{1/4} = 144.3$ MeV $m_{\rm s} = 93$ MeV	1	8×10^{-3}–1.4×10^{-2}	6	9	2.0×10^{6}
$a_4 = 0.55$ $T_0 = 10^{10}$ K	13	2.0×10^{-2}–2.6×10^{-2}	13	14	1.9×10^{6}
$\alpha_0 = 10^{-10}$ $\mu_e/\mu_q = 0.1$	18	3.0×10^{-2}–3.6×10^{-2}	18	19	1.9×10^{6}

Notes. The saturation amplitude ranges and equilibrium temperatures are calculated at a pairing gap $\Delta = 100$ MeV. Equilibrium temperatures are determined using the energy balance Equation (17).
[a] $P_{\rm min}$ is obtained at an age of 2000 yr with a pairing gap $\Delta = 5$ MeV.
[b] $P_{\rm max}$ is obtained at an age of 6000 yr with a pairing gap $\Delta = 200$ MeV.

modes are unstable and can grow. The close overlap of the instability boundaries for different Δ indicates that the *r*-mode instability window is only weakly sensitive to the pairing gap.

This weak dependence arises because the dominant damping mechanism, shear viscosity, is primarily controlled by electron-electron scattering. Its temperature dependence, $\propto T^{\frac{5}{3}}$, does not vary significantly with Δ within the parameter range we considered, as shown in Equation (13). In contrast, bulk viscosity is strongly suppressed in the CFL phase and plays a negligible role in *r*-mode damping (Alford et al. 2008). The detailed shape of the instability window also depends on EoS. The error bar in Figure 2(b) indicates the internal temperature inferred from the observed surface temperature, highlighting the connection between observable quantities and internal properties of the star.

The critical frequency $\nu_{\rm c}$ delineates the transition between stable and unstable regimes. If the stellar spin frequency is below $\nu_{\rm c}$, viscous damping dominates, and *r*-modes are suppressed. Conversely, if the spin frequency exceeds $\nu_{\rm c}$, gravitational wave emission drives *r*-mode growth, resulting in angular momentum loss and heating. Thus, $\nu_{\rm c}$ is an essential quantity in evaluating the influence of *r*-mode activity on the thermal and rotational evolution of the star. To provide a useful tool for further analysis and comparison, we derive a semi-analytical expression for the critical frequency $\nu_{\rm c}$, as a function of internal temperature T:

$$\nu_c \approx -29.8 \log T + 280.4 \text{ Hz}. \quad (14)$$

This empirical fit is based on numerical results shown in Figure 2(b) and is valid over the temperature range $T \approx 10^7$–10^9 K. The fitting accuracy is typically within 10% across this range. From the observed redshifted surface temperature of XMMU J1732, we obtain a critical frequency of $\nu_{\rm c} = 22.25^{+1.24}_{-1.24}$ Hz ($P_{\rm c} = 44.94^{+4.49}_{-4.49}$ ms). The corresponding *r*-mode heating rate is estimated to be $H_{\rm sv} = 1.27 \times 10^{34}$ erg s^{-1}, which is consistent with the observed thermal luminosity of $10.8^{+3.7}_{-3} \times 10^{33}$ erg s^{-1} (Doroshenko et al. 2022). This consistency supports the interpretation that *r*-mode heating is the dominant mechanism sustaining the observed surface temperature of XMMU J1732.

3.3. Thermal Evolution of XMMU J1732

Figure 3(a) presents the thermal evolution curves for six different values of the pairing gap, with and without *r*-mode heating. The pairing gap significantly affects the cooling behavior during the first $\sim$100 yr by modulating neutrino emissivity. Beyond this stage, when photon emission becomes the dominant cooling mechanism, the surface temperature curves corresponding to different Δ values converge. At an age of 4 kyr, the spread in surface temperature predictions across the full range $\Delta = 5$–200 MeV is less than approximately 15% for a fixed saturation amplitude $\alpha_{\rm sat}$.

As shown in Figure 3(a), in the absence of *r*-mode heating (lower set of curves), the star cools rapidly and fails to reproduce the observed surface temperature. When *r*-mode heating is included (upper set of curves), the model successfully reproduces the observed temperature range of XMMU J1732. During the early evolutionary state ($t \lesssim 100$ yr), cooling is dominated by neutrino emission, which is highly sensitive to the pairing gap Δ. At later times, photon emission becomes the dominant cooling mechanism, and the dependence on Δ decreases to below 5%.

The thermal evolution of XMMU J1732 can be explained by *r*-mode heating, where the heating power is governed by the saturation amplitude $\alpha_{\rm sat}$. A higher $\alpha_{\rm sat}$ corresponds to more efficient dissipation of rotational energy, resulting in a higher internal temperature and slower cooling. The appearance of a temperature plateau in the *r*-mode heated curves reflects a quasi-equilibrium state, where heating from *r*-modes balances surface photon emission. The equilibrium temperature is thus set by the magnitude of $\alpha_{\rm sat}$.

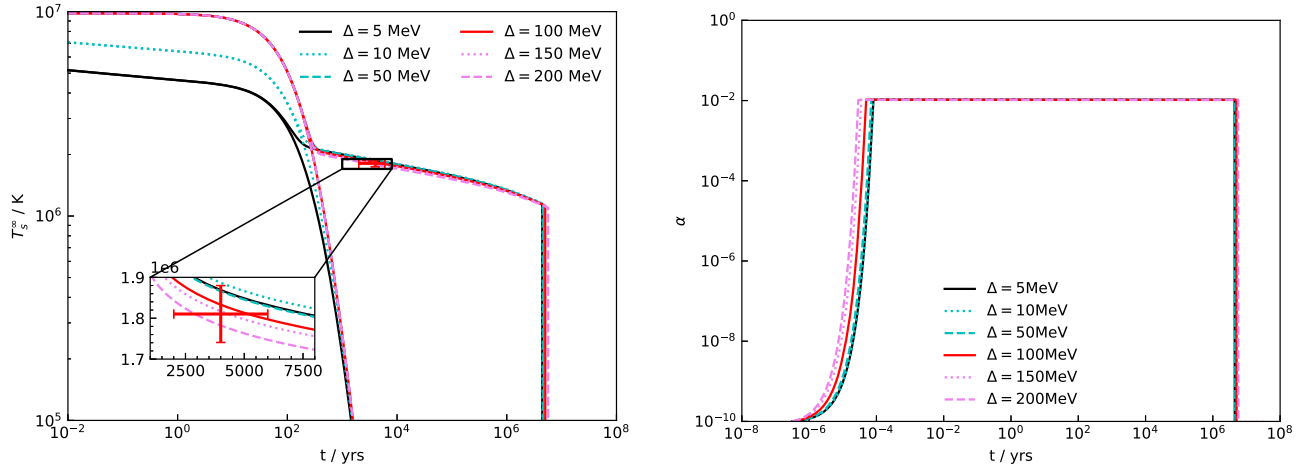

(a) (b)

Figure 3. Thermal and r-mode amplitude evolution for $P_0 = 1$ ms and $\alpha_{\rm sat} = 10^{-2}$. (a) Thermal evolution curves for different pairing gaps (Δ). Flattened segments correspond to quasi-equilibrium maintained by r-mode heating. The error bar indicates the observed surface temperature $T_{\rm s}^{\infty} = 1.81^{+0.07}_{-0.07} \times 10^6$ K (156^{+6}_{-6} eV) and age range 2–6 kyr of XMMU J1732. (b) Evolution of r-mode amplitude, showing rapid saturation across all Δ values.

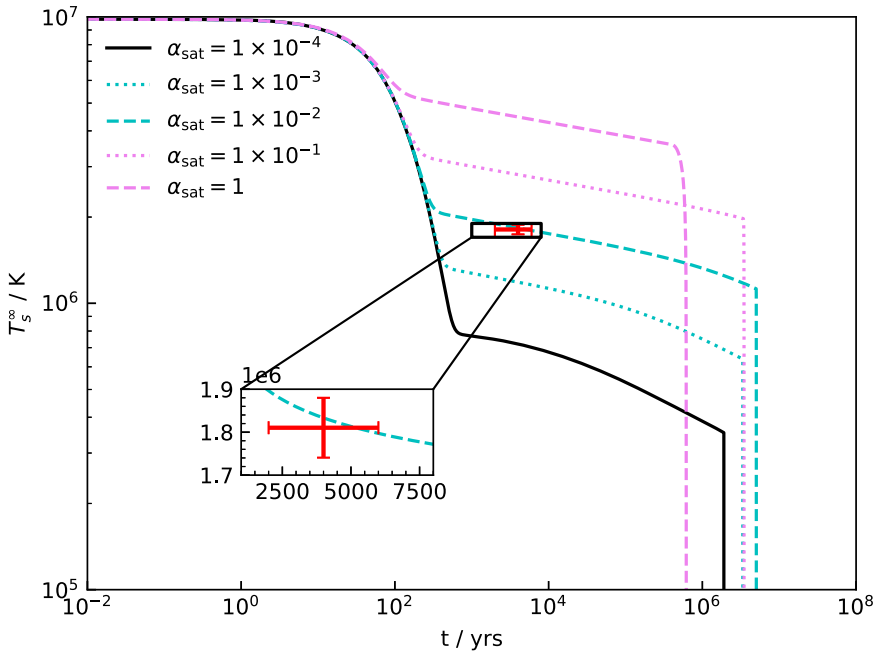

Figure 4. Thermal evolution curves for different saturation amplitudes ($\alpha_{\rm sat}$), with $P_0 = 1$ ms and $\Delta = 100$ MeV. The error bar represents the observed surface temperature $T_{\rm s}^{\infty} = 1.81^{+0.07}_{-0.07} \times 10^6$ K (156^{+6}_{-6} eV) and age 2–6 kyr of XMMU J1732.

Figure 3(b) shows that the r-mode amplitude reaches its saturation value within a few years after the star's birth and remains nearly constant thereafter. Figure 4 shows how $\alpha_{\rm sat}$ determines the equilibrium temperature through the balance between r-mode heating and surface photon cooling. We adopt $\Delta = 100$ MeV as our reference value, representative of a moderate pairing scenario. Since thermal evolution becomes nearly insensitive to Δ after $\sim$100 yr (with variations less than 5%), this choice is sufficient to constrain $\alpha_{\rm sat}$. The observed temperature range provides direct limits on $\alpha_{\rm sat}$, yielding bounds of approximately 8×10^{-3}–1.4×10^{-2} for $P_0 = 1$ ms.

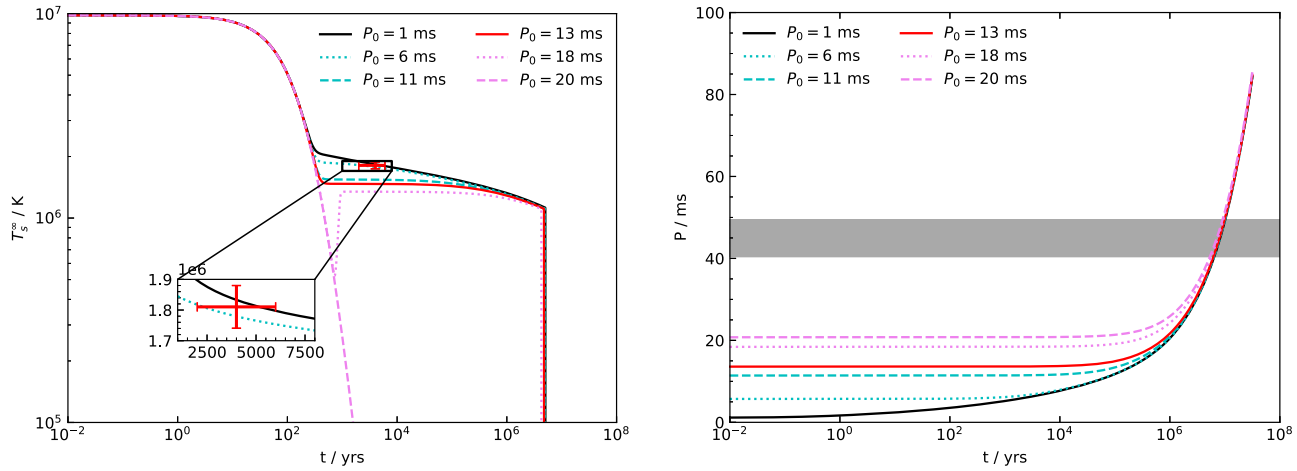

(a) (b)

Figure 5. Thermal and spin evolution curves for different initial periods with $\alpha_{\rm sat} = 10^{-2}$ and $\Delta = 100$ MeV. (a) Thermal evolution curves showing that r-mode heating becomes ineffective for initial periods exceeding 18 ms. The error bar indicates the observed surface temperature $T_s^\infty = 1.81^{+0.07}_{-0.07} \times 10^6$ K (156^{+6}_{-6} eV) and age 2–6 kyr of XMMU J1732. (b) Spin evolution curves for different initial periods. The gray shaded area represents the stability boundary defined by the critical period $P_c = 44.94^{+4.49}_{-4.49}$ ms from Equation (14).

We also test the effects of different initial spin periods. Figure 5 shows that for $P_0 \gtrsim 18$ ms, r-mode heating becomes ineffective as the star quickly spins down below the critical frequency, stabilizing the r-mode. Consequently, sustaining the observed temperature requires a relatively rapid initial rotation ($P_0 \lesssim 18$ ms). Based on this constraint, we examine models with $P_0 = 1$, 13 and 18 ms.

Figure 5(b) shows the spin evolution for various P_0 corresponding to the stable regime below the critical period $P_c = 44.94^{+4.49}_{-4.49}$ ms (from Equation (14)). Stars born with $P_0 \gtrsim 18$ ms quickly cross into the stable regime and cease r-mode heating (as shown in Figure 5(a)). In contrast, shorter initial periods provide a larger rotational energy reservoir, enabling prolonged heating.

Using the observational constraints on surface temperature and age, we estimate the current spin period of XMMU J1732 by scanning across $\Delta = 5$–200 MeV. The resulting ranges for spin period and equilibrium temperature are summarized in Table 2.

3.4. Quasi-equilibrium Temperature and Constraints on R-mode Parameters

In the CFL phase, neutrino emission is significantly suppressed due to quark pairing. As the star evolves and the r-mode amplitude reaches its saturation value, the system enters a quasi-equilibrium state in which the thermal evolution is governed by the balance between r-mode heating and surface photon emission. This balance determines the quasi-equilibrium surface temperature of the star and can be written as:

$$H_{\rm sv} = L_{\rm photon}, \tag{15}$$

where the surface photon luminosity is given by:

$$L_{\rm photon} = 4\pi R^2 \sigma T_s^4 = 4\pi R^2 \sigma (T_s^\infty)^4 (1 - r_g/R)^{-2}. \tag{16}$$

where σ is the Stefan–Boltzmann constant and $r_g = 2GM/c^2$ is the gravitational radius.

Substituting the expressions for $H_{\rm sv}$ (Equation (12)) and $L_{\rm photon}$ (Equation (16)), and the shear viscosity timescale $\tau_{\rm sv}$ due to electron-electron scattering (Equation (13)), and using the known parameters for XMMU J1732 ($\tilde{J} \approx 0.033$, $M = 1.53 \times 10^{33}$ g, $R = 1.04 \times 10^6$ cm, $\mu_e/\mu_q \approx 0.1$ (calculated from the EoS in Section 3.1), we derive the following relation for the redshifted surface temperature as a function of the r-mode saturation amplitude and angular velocity:

$$T_s^\infty \approx 9.3 \times 10^5 (\alpha_{\rm sat}\,\Omega)^{0.28}\ {\rm K}. \tag{17}$$

This expression reveals that a larger r-mode amplitude and/or a higher spin rate result in stronger r-mode heating, leading to an increased equilibrium surface temperature. This relationship is illustrated in Figure 4.

Using the observed surface temperature $T_s^\infty = 1.81 \times 10^6$ K for XMMU J1732, we find:

$$\alpha_{\rm sat}\,\Omega \approx 10.8\ {\rm rad\ s^{-1}}. \tag{18}$$

Expressing the angular velocity in terms of the spin period ($\Omega = 2\pi/P$), we derive a direct relation between the r-mode

saturation amplitude and the spin period:

$$\alpha_{\rm sat} \approx 1.7 \times 10^{-3}\left(\frac{P}{\rm ms}\right). \quad (19)$$

Equation (19) provides a quantitative link between the thermal and rotational evolution of the star. As discussed in Section 3.3, we consider a range of initial spin periods, which lead to different constraints on $\alpha_{\rm sat}$. The inferred values are broadly consistent with theoretical expectations from nonlinear mode coupling models, which predict saturation amplitudes in the range $\alpha_{\rm sat} \sim 10^{-4}$–$10^{-2}$ (Bondarescu et al. 2009). This range reflects the complex nonlinear interactions among fluid modes that naturally limit the amplitude of *r*-mode oscillations to values well below unity. The consistency between our model predictions and theoretical estimates supports the role of *r*-mode heating as the mechanism sustaining the thermal luminosity of XMMU J1732.

Moreover, Equation (19) provides a testable prediction. A future detection of coherent pulsations from XMMU J1732 would allow a direct measurement of its spin period, and allow empirical validation of the inferred $\alpha_{\rm sat}$–P relation. Confirmation of this relation would further support the *r*-mode heating scenario and strengthen the case for interpreting XMMU J1732 as a CFL strange star. Conversely, a significant discrepancy would imply the need to revise either the assumed saturation mechanism or the underlying microphysical properties of the dense matter phase.

4. Conclusions and Discussion

In this work, we present a detailed thermal evolution model for the central compact object XMMU J1732, located in the supernova remnant HESS J1731−347. Our model includes *r*-mode heating in a self-consistent CFL phase strange star. This approach extends earlier studies that mainly focused on mass–radius constraints. We directly connect the thermal properties of XMMU J1732 to microscopic parameters that govern the CFL phase and *r*-mode instability. This allows for a more complete understanding of this unusual object. Our thermal evolution model, which includes *r*-mode heating in a CFL strange star, successfully explains the observed high temperature and low mass of XMMU J1732. This makes it a strong alternative to standard neutron star models.

Our results suggest that *r*-mode heating is the main internal heat source in young compact stars with CFL quark matter cores. We constrain the *r*-mode saturation amplitude $\alpha_{\rm sat}$ to be between 8×10^{-3} and 1.4×10^{-2} for an initial spin period of 1 ms. This range agrees with theoretical predictions from mode coupling studies (Bondarescu et al. 2009). We also constrain the initial spin period P_0 to be less than about 18 ms. If the star had spun more slowly at birth, it would have cooled too quickly through *r*-mode emission to match the observed thermal properties. Our model predicts a current spin period of 6–9 ms for XMMU J1732. This rapid rotation is consistent with the lack of detected pulsations, which may result from unfavorable viewing geometry or weak pulsed emission (Lorimer 2005; Faucher-Giguere & Kaspi 2006; Wu et al. 2021).

The predicted rapid spin of XMMU J1732 sets it apart from other CCOs. Only four CCOs have currently measured spin periods and period derivatives, and all of them rotate much more slowly, with periods around 0.1 s (Halpern & Gotthelf 2015; Gotthelf et al. 2024). This difference may reflect variations in initial spin periods, saturation amplitudes, magnetic fields, or the EoS. Finding a rapidly rotating CCO would have important implications for our understanding of CCO evolution and the physics of dense matter. Future comparisons of thermal and spin properties across the CCO population will be important for addressing these questions.

While our model provides a self-consistent explanation for XMMU J1732, it relies on several simplifying assumptions. We assume spherical symmetry and a uniform internal temperature. These assumptions can affect thermal transport, potentially introducing deviations in the equilibrium temperature estimate. Detailed studies of anisotropic temperature distributions in neutron stars with magnetic fields (Geppert et al. 2004; Aguilera et al. 2008) have shown that surface temperature variations of 10%–15% are typical when comparing 2D models to spherically symmetric ones. Potekhin et al. (2015) further confirmed that internal temperature gradients can modify the overall thermal evolution by similar amounts. Since *r*-mode heating is distributed throughout the star, rather than confined to localized regions, the overall impact of these simplifications on our main conclusions is expected to be limited to corrections of this magnitude.

We have also considered the effect of magnetic fields. For XMMU J1732, the inferred field strength is $B \sim 10^{11}$ G, typical of CCOs. The results in Wang & Dai (2017) suggest that such fields modify *r*-mode damping timescales by less than 5%. Including magnetic effects would improve quantitative accuracy but is unlikely to change the qualitative results. Future studies incorporating magnetic damping mechanisms (Rezzolla et al. 2000; Ho & Lai 2000; Glampedakis et al. 2006) and improved modeling of the EoS of CFL phase quark matter will further refine the results.

Future observations will be the key factor in testing and refining our model. Continued efforts to detect radio emission or place tighter constraints on the pulsed fraction are important for confirming the predicted rapid rotation. High-precision timing observations with next-generation facilities offer a promising way for achieving these goals and potentially measuring the spin period directly. Although the direct detection of gravitational waves from *r*-mode remains a significant challenge, future advances in detector sensitivity (e.g., with third-generation detectors like Cosmic Explorer and Einstein Telescope) might eventually make this possible,

providing a direct probe of the *r*-mode mechanism and the internal dynamics of these compact objects.

In conclusion, our results support the identification of XMMU J173203.3−344518 as a rapidly rotating CFL strange star heated by *r*-mode dissipation. This model explains the unusual properties of the object, constrains key parameters such as the *r*-mode amplitude and initial spin period, and offers a new path to study dense matter in extreme environments. These findings show that *r*-mode may play an important role in the early thermal and spin evolution of compact stars and emphasize the need for continued observational and theoretical investigations to the nature of these kinds of compact objects.

Acknowledgments

We would like to thank the anonymous referee for helpful suggestions that led to significant improvement of our study. This work is supported in part by the Natural Science Foundation of Xinjiang Uygur Autonomous Region (No. 2023D01E20), the National Key R&D Program of China (No. 2022YFA1603104), the National Natural Science Foundation of China (Nos. 12288102, 12273028 and 12033001), the Tianshan talents program (2023TSYCTD0013), the Major Science and Technology Program of Xinjiang Uygur Autonomous Region (No. 2022A03013-1) and the Urumqi Nanshan Astronomy and Deep Space Exploration Observation and Research Station of Xinjiang (XJYWZ2303).

References

Abbott, B. P., Abbott, R., Abbott, T. D., et al. 2018, PhRvL, 121, 161101
Aguilera, D. N., Pons, J. A., & Miralles, J. A. 2008, A&A, 486, 255
Alford, M. 2001, ARNPS, 51, 131
Alford, M., Braby, M., Paris, M., & Reddy, S. 2005, ApJ, 629, 969
Alford, M. G., Schmitt, A., Rajagopal, K., & Schäfer, T. 2008, RvMP, 80, 1455
Alford, M., Rajagopal, K., & Wilczek, F. 1999, NuPhB, 537, 443
Andersson, N. 1998, ApJ, 502, 708
Andersson, N., Jones, D., & Kokkotas, K. 2002, MNRAS, 337, 1224
Atta, D., & Basu, D. 2025, Prama, 99, 38
Blaschke, D., Klähn, T., & Voskresensky, D. 2000, ApJ, 533, 406
Bondarescu, R., Teukolsky, S. A., & Wasserman, I. 2009, PhRvD, 79, 104003
Brown, E. F. 1999, The thermal and compositional structure of the crust of an accreting neutron star, ProQuest Dissertations and Theses, University of California, Berkeley
Chandrasekhar, S. 1970, PhRvL, 24, 611
Choudhury, D., Salmi, T., Vinciguerra, S., et al. 2024, ApJL, 971, L20
Cui, Y., Pühlhofer, G., & Santangelo, A. 2016, A&A, 591, A68
de Luca, A. 2008, in AIP Conf. Ser. 983, 40 Years of Pulsars: Millisecond Pulsars, Magnetars and More, ed. C. Bassa et al. (Melville, NY: AIP), 311
Di Clemente, F., Drago, A., & Pagliara, G. 2024, ApJ, 967, 159
Doroshenko, V., Suleimanov, V., Pühlhofer, G., & Santangelo, A. 2022, NatAs, 6, 1444
Du, S.-S., Liu, X.-J., Chen, Z.-C., et al. 2024, ApJ, 968, 105
Faucher-Giguere, C. A., & Kaspi, V. M. 2006, ApJ, 643, 332
Friedman, J. L., & Schutz, B. F. 1978, ApJ, 222, 281
Geppert, U., Küker, M., & Page, D. 2004, A&A, 426, 267
Glampedakis, K., Samuelsson, L., & Andersson, N. 2006, MNRAS, 371, L74
Gotthelf, E., Perez, K., & Halpern, J. 2024, AAS/High Energy Astrophysics Division, 21, 107
Gotthelf, E. V., Halpern, J. P., & Alford, J. 2013, ApJ, 765, 58
Group, P. D., Workman, R., Burkert, V., et al. 2022, PTEP, 2022, 083C01
Gudmundsson, E. H., Pethick, C., Epstein, R. I., et al. 1983, ApJ, 272, 286
Halpern, J., & Gotthelf, E. 2015, ApJ, 812, 61
Ho, W. C., & Lai, D. 2000, ApJ, 543, 386
Horvath, J., Rocha, L., de Sá, L., et al. 2023, A&A, 672, L11
Huang, H.-t., Zhou, X., Yuan, J.-p., & Zheng, X.-P. 2022, MNRAS, 512, 4689
Iwamoto, N. 1982, AnPhy, 141, 1
Kurkela, A., Rajagopal, K., & Steinhorst, R. 2024, PhRvL, 132, 262701
Laskos-Patkos, P., Koliogiannis, P., & Moustakidis, C. C. 2024, PhRvD, 109, 063017
Lattimer, J. 2021, ARNPS, 71, 433
Li, A., Miao, Z.-Q., Jiang, J.-L., Tang, S.-P., & Xu, R.-X. 2021, MNRAS, 506, 5916
Li, X.-D., Bombaci, I., Dey, M., Dey, J., & Van Den Heuvel, E. 1999, PhRvL, 83, 3776
Liu, H.-M., Chu, P.-C., Liu, H., Li, X.-H., & Li, Z.-H. 2025, arXiv:2501.04382
Lorimer, D. R. 2005, LRR, 8, 7
Lorimer, D. R. 2008, LRR, 11, 8
Lyne, A. G., Pritchard, R. S., & Graham Smith, F. 1993, MNRAS, 265, 1003
Miller, M. C., Lamb, F., Dittmann, A., et al. 2021, ApJL, 918, L28
Miller, M., Lamb, F. K., Dittmann, A., et al. 2019, ApJL, 887, L24
Oikonomou, P., & Moustakidis, C. C. 2023, PhRvD, 108, 063010
Owen, B. J., Lindblom, L., Cutler, C., et al. 1998, PhRvD, 58, 084020
Potekhin, A. Y., Pons, J. A., & Page, D. 2015, SSRv, 191, 239
Rezzolla, L., Lamb, F. K., & Shapiro, S. L. 2000, ApJ, 531, L139
Riley, T. E., Watts, A. L., Bogdanov, S., et al. 2019, ApJL, 887, L21
Riley, T. E., Watts, A. L., Ray, P. S., et al. 2021, ApJL, 918, L27
Sagun, V., Giangrandi, E., Dietrich, T., et al. 2023, ApJ, 958, 49
Salmi, T., Choudhury, D., Kini, Y., et al. 2024, ApJ, 974, 294
Sun, Y., Wang, D., Zhang, C., et al. 2024, ARep, 68, 268
Suwa, Y., Yoshida, T., Shibata, M., Umeda, H., & Takahashi, K. 2018, MNRAS, 481, 3305
Viganò, D., Rea, N., Pons, J. A., et al. 2013, MNRAS, 434, 123
Wang, J.-S., & Dai, Z.-G. 2017, A&A, 603, A9
Wang, Y.-B., Zhou, X., Wang, N., & Liu, X.-W. 2019, RAA, 19, 030
Wang, Z., Kaplan, D. L., & Chakrabarty, D. 2007, ApJ, 655, 261
Weissenborn, S., Sagert, I., Pagliara, G., Hempel, M., & Schaffner-Bielich, J. 2011, ApJL, 740, L14
Witten, E. 1984, PhRvD, 30, 272
Wu, Q., Pires, A. M., Schwope, A., et al. 2021, RAA, 21, 294
Zhang, S.-R., Hernandez, J. R., & Negreiros, R. 2024, ApJ, 978, 1
Zheng, X.-P., Yu, Y.-W., & Li, J.-R. 2006, MNRAS, 369, 376
Zhou, E.-P., Zhou, X., & Li, A. 2018, PhRvD, 97, 083015
Zhou, X., Li, A., & Li, B.-A. 2021, ApJ, 910, 62